JPET Fast Forward. Published on August 10, 2005 as DOI: 10.1124/jpet.105.090928
This article has not been copyedited and formatted. The final version may differ from this version.

Title:

Enantiomer/Enantiomer Interactions between the *S*- and *R*- Isomers of Omeprazole in Human Cytochrome P450 Enzymes: Major Role of CYP2C19 and CYP3A4

Author:

Xue-Qing Li, Lars Weidolf, Roger Simonsson and Tommy B. Andersson

Institution:

DMPK and Bioanalytical Chemistry (X-Q.L., L.W., T.B.A.) and Medicinal Chemistry (R.S.), AstraZeneca R&D Mölndal, Sweden

Division of Molecular Toxicology, Institute of Environmental Medicine, Karolinska Institutet, Stockholm, Sweden (T.B.A.)

JPET Fast Forward. Published on August 10, 2005 as DOI: 10.1124/jpet.105.090928
This article has not been copyedited and formatted. The final version may differ from this version.

Running Title: Enantiomer interactions of *S*- and *R*-Omeprazole on P450s

Corresponding author: Xue-Qing Li, PhD

Postal address:

DMPK and Bioanalytical Chemistry

AstraZeneca R&D Mölndal

S-431 83 Mölndal

Sweden

Telephone: +46-31-706 5506

Fax number: +46-31-776 3786

E-mail address: Xueqing.Li@astrazeneca.com

Text statistics:

The number of Pages: 35

The number of Tables: 2

The number of Figures: 8

The number of References: 30

The number of words in the Abstract: 223

The number of words in the Introduction: 650

The number of words in the Discussion: 1430

Abbreviations used:

PPIs, proton pump inhibitors; HLM, human liver microsomes; P450, cytochrome P450; recombinant P450 2C19, rCYP2C19; recombinant P450 3A4, rCYP3A4; LC/MS/MS, liquid chromatography-tandem mass spectrometry; SRM, selected reaction monitoring; OME, racemic omeprazole; *S*-OME, the *S*-enantiomer of omeprazole; *R*-OME, the *R*-enantiomer of omeprazole; OH-OME, hydroxyomeprazole; RAF, relative activity factor; EM, extensive metabolizer; PM, poor metabolizer; K_i, apparent inhibition constant; CL_{int}, intrinsic clearance. V_{max}, K_m, and v all refer to the enzyme kinetic parameters of individual enantiomers; apparent $V_{\max}^{app}$, K_m^{app}, and v^{app} all refer to the enzyme kinetic parameters of enantiomers in racemate.

Recommended section assignment: Absorption, Distribution, Metabolism, and Excretion Behavioral Pharmacology

JPET Fast Forward. Published on August 10, 2005 as DOI: 10.1124/jpet.105.090928
This article has not been copyedited and formatted. The final version may differ from this version.

ABSTRACT

We investigated the enzyme kinetic basis for the stereoselective disposition of *R*- and *S*-omeprazole (OME) and racemic OME in human liver microsomes. OME is primarily metabolized by the hepatic cytochrome P450 enzyme system (CYP2C19 and 3A4). The metabolism of each enantiomer and pseudoracemic OME was studied using unlabelled and $^{13}C_7$-labelled enantiomers. The enantiomers inhibited each other's metabolism competitively in human liver microsomes and in recombinant CYP2C19 and 3A4. The results obtained with the individual enantiomers allowed successful prediction of the enzyme kinetics for the pseudoracemate. The intrinsic clearance of each enantiomer in a pseudoracemic mixture remained the same as those of the individually incubated enantiomers, although K_m and V_{max} decreased. In the pseudoracemate, the relative contribution of CYP2C19 and 3A4 to 5-hydroxylation and 5'-*O*-demethylation of *R*-OME was comparable with that obtained for incubation of *R*-OME alone. For *S*-OME, however, the presence of its antipode greatly increased the contribution of CYP3A4, with increasing concentrations, compared with that obtained when incubating *S*-OME alone. The results of our in vitro study clearly show metabolic interactions between the OME enantiomers, which may also occur in vivo. Because the enantiomers of OME produce similar pharmacological effects, the enantiomer interactions should not significantly affect the pharmacodynamics. On the other hand, the use of the *S*-enantiomer results in less complex enzyme kinetics than those of the racemate and, thus, the outcome of its clinical use is more predictable.

INTRODUCTION

Omeprazole (OME), a proton pump inhibitor (PPI), has been widely used for many years as an acid inhibitory agent for the treatment of gastric acid hypersecretion disorders. OME is a chiral compound and the sulfinyl group is the chiral center (Fig.1). It is administered as a racemic (50/50) mixture of the *S*- and *R*-enantiomers. Recently its optical *S*-isomer has been developed as a new drug (esomeprazole). OME, as well as its enantiomers, are prodrugs with a common mechanism of action involving chemical rearrangement to a pharmacologically active achiral sulfenamide in the acidic compartment of parietal cells (Lindberg et al., 1986). The formed sulfenamide reacts with sulfhydryl groups of the enzyme H^+,K^+-ATPase (the proton pump), which is located in the canaliculi of the parietal cells, thus inhibiting its ability to participate in gastric acid formation. OME and its enantiomers are thus equally potent H^+,K^+-ATPase inhibitors (Andersson et al., 2001). However, *R*- and *S*-OME show stereoselective disposition because of the enzyme-catalyzed stereoselective metabolism that lead to the higher metabolic stability of esomeprazole compared with its *R*-isomer and the racemate, which has been demonstrated in vitro using human liver microsomes (Äbelö et al., 2000). The resulting increase in drug exposure in the majority of the population, as indicated by the higher area under the plasma concentration-time curve (AUC) after esomeprazole administration, provides more effective control of gastric acid secretion than that of the other PPIs (lansoprazole, pantoprazole and rabeprazole) when given at their standard doses (Lindberg et al., 2003; Miner et al., 2003).

JPET Fast Forward. Published on August 10, 2005 as DOI: 10.1124/jpet.105.090928
This article has not been copyedited and formatted. The final version may differ from this version.

OME and its enantiomers are extensively metabolized in the liver by the cytochrome P450 (P450) enzyme system and the major metabolites formed are 5'-*O*-desmethylOME, 5- and 3-hydroxyOME (5- and 3-OH-OME), and OME sulfone (Renberg et al., 1989; Andersson et al., 2001) (Fig. 1). These metabolites do not contribute to the pharmacological effect (Data on file). Formation of the sulfone metabolite and 3-OH-OME is mediated by CYP3A4, whereas 5-OH-OME and 5'-*O*-desmethylOME are mainly formed by CYP2C19 with some contribution from CYP3A4. Previous in vitro studies have shown that *R*-OME is cleared efficiently via CYP2C19 with minor contribution from CYP3A4, while the reverse P450 contribution was found for the *S*-isomer but with relatively lower clearance (Äbelö et al., 2000). This difference in enzyme kinetic properties between the two enantiomers in vitro is in agreement with stereoselective pharmacokinetics of the OME enantiomers in vivo (Tybring et al., 1997). The total system clearance (*CL/F*) of *R*-OME was approximately 1.4-fold higher than for *S*-OME after oral administration of racemic OME in CYP2C19 extensive metabolizers (EMs). In another study, the total system clearance of *R*-OME was 1.9-fold higher than that for *S*-OME in EMs, after separate oral administration of *R*- and *S*-OME (Andersson et al., 2001). This difference in pharmacokinetic and enzyme kinetic characteristics prompted us to investigate the enantiomer/enantiomer interactions between *R*- and *S*-OME in detail using current in vitro technologies.

The aim of this work was to characterize the interactions between the enantiomers of OME, with respect to their four metabolic reactions. A detailed investigation of the enantiomer/enantiomer interactions on the formation rates of OME enantiomer metabolites and the contribution of individual P450

JPET Fast Forward. Published on August 10, 2005 as DOI: 10.1124/jpet.105.090928
This article has not been copyedited and formatted. The final version may differ from this version.

enzymes was made possible by using *S*-[$^{13}C_7$]OME and unlabeled *R*-OME and subsequently, LC/MS/MS analysis. A thorough analysis was made of the enzyme reactions according to kinetic models describing competition of enzyme activities towards a racemic mixture when the enantiomers are substrates to the same enzymes. Because racemic OME is used clinically, in vitro catalytic data on the racemic substrate and the individual enantiomers can be used to explain the in vitro-in vivo correlation of the metabolism of OME reported in humans. The maximum plasma concentrations after therapeutically relevant repeated doses of OME racemate in CYP2C19 EMs and poor metabolizers (PMs) were 1 and 3 μM, respectively, and 5 and 7 μM of esomeprazole in EMs and PMs, respectively (Li et al., 2004). Thus, this clinically relevant substrate concentration range has been included in our study.

JPET Fast Forward. Published on August 10, 2005 as DOI: 10.1124/jpet.105.090928
This article has not been copyedited and formatted. The final version may differ from this version.

MATERIALS AND METHODS

Chemicals and Reagents. Racemic OME sodium (*rac*-5'-methoxy-2'-[[(4-methoxy-3,5-dimethyl-2-pyridinyl)methyl]sulfinyl]-1*H*-benzimidazole sodium salt) was obtained from AstraZeneca Bulk Production (Södertälje, Sweden). *S*-OME sodium, and *R*-OME sodium were obtained from AstraZeneca Process R&D (Södertälje, Sweden). *S*-[$^{13}C_7$]OME potassium (see Fig.1 for the positions of the ^{13}C-labels, the full synthesis description can be found online as *Supplemental data*), OME sulfone (5'-methoxy-2'-[[(4-methoxy-3,5-dimethyl-2-pyridinyl)methyl]sulfonyl]-1*H*-benzimidazole), and racemic 5'-*O*-desmethylOME (*rac*-5'-hydroxy-2'-[[(4-methoxy-3,5-dimethyl-2-pyridinyl)methyl]sulfinyl]-1*H*-benzimidazole) were obtained from Medicinal Chemistry (AstraZeneca R&D Mölndal, Sweden). Racemic 5-OH-OME (*rac*-5'-methoxy-2'-[[(4-methoxy-3-methyl-5-hydroxymethyl-2-pyridinyl)methyl]sulfinyl]-1*H*-benzimidazole) was obtained from Synthelec AB (Lund, Sweden). Tinidazole (internal standard) and reduced nicotinamide adenine dinucleotide phosphate (NADPH) were purchased from Sigma Chemical Co. (St. Louis, MO). The enantiomeric purity of each OME enantiomer was >99%. All other chemicals and reagents were of the highest commercially available quality.

Human Liver Microsomes (HLM) and Recombinant Cytochrome P450s. Human liver samples (excess liver tissue removed during surgery on the liver) were obtained from Sahlgrenska Hospital, Göteborg, Sweden. All tissues were obtained by qualified medical staff, with donor consent and with the approval of the local ethics committee at Sahlgrenska Hospital. HLM were prepared from 20 liver samples obtained from male and female patients

JPET Fast Forward. Published on August 10, 2005 as DOI: 10.1124/jpet.105.090928
This article has not been copyedited and formatted. The final version may differ from this version.

(Caucasian) according to the method of Ernster et al. (Ernster et al., 1962). A pool was prepared by mixing equal volumes of each individual liver microsomal preparation, with similar protein content, to reflect the average P450 activities in humans. Recombinant human CYP2C19 and 3A4 (rCYP2C19 and rCYP3A4) were heterologously expressed in *Saccharomyces cerevisiae* and obtained from AstraZeneca Biotech Laboratory (Södertälje, Sweden) (Masimirembwa et al., 1999). Microsomal protein concentration was measured according to Lowry et al. (Lowry et al., 1951) using bovine serum albumin as the standard. The microsomal preparations were stored at –80°C until use.

Incubation of omeprazole enantiomers and pseudoracemate with HLMs and rCYP2C19 and 3A4. The in vitro incubation system consisted of HLM (0.3 mg/ml of protein, or rCYP2C19/3A4 with 50 pmol/ml), OME *R*- and *S*-enantiomers or the mixture of equal or unequal mole fractions of *S*-[$^{13}C_7$]OME and *R*-OME, and 1 mM NADPH dissolved in 0.1 M Tris-hydrochloride buffer (pH 7.4) in a final volume of 200 µl. All incubations were conducted at 37°C for 20 min. Linear conditions for the formation rate of 5- and 3-OH-OME, 5'-*O*-desmethylOME and OME sulfone were evaluated with respect to protein content and incubation time. The optimum conditions, as described above, were selected for the kinetic study. All reactions were performed in 96-well plates. The metabolic reactions were started by addition of NADPH after a preincubation of 5 min at 37°C, and terminated by the addition of an aliquot of 100 µl ice-cold acetonitrile (containing 1.5 µM internal standard). After centrifugation at 4,500 *g* for 20 min, 20 µl of supernatant was injected into the LC/MS/MS system. Samples were quantified by monitoring

JPET Fast Forward. Published on August 10, 2005 as DOI: 10.1124/jpet.105.090928
This article has not been copyedited and formatted. The final version may differ from this version.

the ratio between the metabolites of the enantiomers of OME and the internal standard in each sample and in calibration curves. All incubations throughout the study were carried out in duplicate. For each incubation, the test compounds were dissolved in methanol and sequentially diluted with 40% of methanol in 0.1 M tris-hydrochloride buffer (pH 9). The final pH value of the incubation mixture was kept at 7.4 and the methanol concentration was less than 1%.

The formation kinetics of 5'-*O*-desmethylOME, 5- and 3-OH-OME and OME sulfone were determined at substrate concentrations ranging from 1 to 128 µM (OME enantiomers and equimolar pseudoracemate). Control experiments excluded unusual enzyme kinetic behavour, especially substrate inhibition, at concentrations up to 750 µM and 400 µM, for rCYP3A4 and rCYP2C19, respectively. The inhibition experiments were performed using *R*-OME as an inhibitor of the metabolism of *S*-[$^{13}C_7$]OME, and vice versa. The substrate concentrations were chosen with regard to the Michaelis-Menten kinetics (K_m and V_{max}) for each metabolic reaction (Table 1) (approximately ½ K_m, K_m, 3 K_m and 5 K_m; when two enzyme systems were involved, the high affinity K_{m1} was used). The inhibitor concentrations were varied from 1 to 150 µM at four different concentrations selected on the basis of the IC_{50} values obtained previously (approximately ½×IC_{50}, IC_{50}, 2×IC_{50}, and 4×IC_{50}).

HPLC Conditions. The HPLC system used included a Surveyor MS pump, a built-in degasser, a Surveyor PDA detector (ThermoFinnigan, San Jose, CA, USA) and a CTC HTS autosampler (CTC Analytics, Zwingen, Switzerland). Chromatography was performed on an Eclipse XDB-C8 column (4.6 x 150 mm, 5 µm, Agilent, Palo Alto, CA, USA) with an Eclipse XDB-C8

JPET Fast Forward. Published on August 10, 2005 as DOI: 10.1124/jpet.105.090928
This article has not been copyedited and formatted. The final version may differ from this version.

guard column (4.6 x 12.5 mm, 5 µm). The mobile phases consisted of (A) 0.1% formic acid in water and (B) 0.1% formic acid in acetonitrile, which increased linearly from 25% of solvent B to 65% B during 5 min at a flow-rate of 0.8 ml/min. The effluent was split with approximately 0.3 ml/min being introduced into the mass spectrometer. The Surveyor PDA detector was set at 302 nm to monitor the consumption of the substrates, which was less than 20 % of their initial concentrations after incubation. The chiral stability of the enantiomers of OME in HLM and rCYP2C19 and 3A4 was also estimated using chiral LC/MS/MS analysis (data not shown). Negligible amounts (< 0.3%) of the optical antipode were detected during incubation of the individual enantiomers of OME at a concentration of 50 µM for 20 min. Thus, the enantiomers of OME are optically stable under the employed experimental conditions in this study.

Mass Spectrometric Conditions. The mass spectrometric analyses were performed using a ThermoFinnigan TSQ Quantum triple quadrupole mass spectrometer (ThermoFinnigan, San Jose, CA, USA). The mass spectrometer was operated in the positive ionization electrospray mode and the instrument settings were optimized using the analytes. The mass spectrometer was operated in the selected reaction monitoring (SRM) mode. The SRM transitions of the $[M + H]^+$ precursor ions to selected product ions were monitored for the analytes and internal standard with the following typical values: 5- and 3-OH-OME, as well as OME sulfone *m/z* 362.1 to 214.0 (collision energy 22 eV); their respective [$^{13}C_7$]-labeled metabolites *m/z* 369.1 to 214.0 (collision energy 22 eV); 5'-*O*-desmethylOME *m/z* 332.1 to 198.0 (collision energy 16 eV); 5'-*O*-[$^{13}C_6$]desmethylOME *m/z* 338.1 to 198.0

JPET Fast Forward. Published on August 10, 2005 as DOI: 10.1124/jpet.105.090928
This article has not been copyedited and formatted. The final version may differ from this version.

(collision energy 16 eV), and internal standard tinidazole *m/z* 248.0 to 121.0 (collision energy 22 eV). Instrument control, data acquisition and data evaluation were performed using Xcalibur software (version 1.3, ThermoFinnigan). Quantitation of [^{13}C]-labeled metabolites was based on the calibration standards prepared by using the unlabelled reference compounds. Because of the lack of synthetic 3-OH-OME standard, the quantitation of this metabolite was evaluated by using 5-OH-OME as the reference. The lower limit of quantification (LLOQ) was 5 nM for all the analytes.

Relative Contributions of CYP2C19 and 3A4 to OME 5'-*O*-Demethylation and 5-Hydroxylation in HLM. Our previous studies demonstrated that CYP2C19 and 3A4 are the major enzymes responsible for 5'-*O*-demethylation and 5-hydroxylation of the OME enantiomers (Äbelö et al., 2000). A relative activity factor (RAF) approach (Crespi, 1995; Störmer et al., 2000) was used to estimate the relative contributions of P450s (RC_i of CYP2C19 and 3A4) on the metabolism of the individual OME enantiomers in HLM, in the absence or presence of the optical antipode. RAF_i values for CYP2C19 (24.8 pmol rCYP2C19/mg HLM) and CYP3A4 (248.1 pmol rCYP3A4/mg HLM) were obtained from our previous study (Li et al., 2003), where they were determined as the ratio of the activity of each enzyme marker reaction in HLM and recombinant P450s. The P450 enzyme specific marker reactions used for CYP2C19 and 3A4 were *S*-mephenytoin 4'-hydroxylation and midazolam 1'-hydroxylation, respectively. The individual $rCYP_i$ reaction velocity $v_{r_i(S)}$ at each substrate concentration, [S], was obtained using the Michaelis-Menten equation (eq. 1). RAF_i values for each respective CYP_i were entered with $v_{r_i(S)}$ in eqs. 2 and 3 to estimate the total

JPET Fast Forward. Published on August 10, 2005 as DOI: 10.1124/jpet.105.090928
This article has not been copyedited and formatted. The final version may differ from this version.

activity in HLM (v) contributed by the CYPs investigated and the relative contribution by each respective CYP_i (RC_i).

$$v_{r_i(S)} = \frac{V_{\max,r_i}[S]}{K_{m,r_i} + [S]} \quad (1)$$

$$v = \sum_i v_{r_i(S)} \times RAF_i \quad (2)$$

$$RC_i(\%) = \frac{v_{r_i(S)} \times RAF_i}{v} \times 100 \quad (3)$$

Enzyme kinetics of *R*- and *S*-enantiomers as competing substrates in a racemic mixture (50:50). The enzyme kinetics for competitive interaction between enantiomers during the metabolism of a pseudoracemic substrate is a special case of competitive inhibition as has been described in detail by Kim et al. (Kim et al., 1993). For a reaction catalyzed by a single enzyme, the apparent Michaelis Menten constants of the *R*- and *S*-enantiomers in a racemic mixture are related to their respective true V_{max} and K_m by an offset containing the ratio of the true K_m values of the enantiomers. This is illustrated by the following equations for the *R*-enantiomer:

$$v_R^{app} = \frac{V_{\max,R}^{app}[R]}{K_{m,R}^{app} + [R]} \quad (4)$$

$$V_{\max,R}^{app} = \frac{V_{\max,R}}{1 + K_{m,R}/K_{m,S}} \quad (5)$$

$$K_{m,R}^{app} = \frac{K_{m,R}}{1 + K_{m,R}/K_{m,S}} \quad (6)$$

$$CL_{m,R}^{app} = \frac{V_{\max,R}^{app}}{K_{m,R}^{app}} = \frac{V_{\max,R}}{K_{m,R}} \quad (7)$$

where [R] is the concentration of the *R*-enantiomer in a racemate. The equations for the *S*-enantiomer in a racemate can be derived in the same

JPET Fast Forward. Published on August 10, 2005 as DOI: 10.1124/jpet.105.090928
This article has not been copyedited and formatted. The final version may differ from this version.

way. Therefore, the apparent $V_{\max}^{app}$ and K_m^{app} of both enantiomers are lower than their respective true values, whereas the clearance of the enantiomers in a racemate is still equal to their true value (eq. 7, i.e. V_{max}/K_m). It can readily be shown that the *R/S* ratio of the apparent K_m^{app} for the enantiomers in a racemate is equal to 1; i.e. $K_{m,R}^{app} = K_{m,S}^{app}$. On the other hand, the values of the *R/S* ratios of the apparent $V_{\max}^{app}$ as well as the metabolite formation velocities (v^{app}) are equal to the ratio of the true intrinsic clearance (i.e. V_{max}/K_m) of the enantiomers. Hence the ratio of the apparent $V_{\max}^{app}$ fully reflects the enantioselectivity of the enzymatic reaction and the v_R^{app}/v_S^{app} ratio is a constant, which is not dependent on the substrate concentration. Deviation from this consistency in the v_R^{app}/v_S^{app} ratio over a range of substrate concentrations may reflect the contribution of multiple enzymes to the formation of a given metabolite with differing K_m values and enantioselectivities.

Data analysis. Enzyme kinetic parameters (K_m, V_{max} and K_i) and inhibition mechanisms were analyzed using non-linear least squares regression by fitting different models of the enzyme kinetic and inhibition data using the SigmaPlot Enzyme Kinetics Module for Windows 7.0 (SPSS, Inc., Chicago, IL). The model with the best fit was selected based on the dispersion of residuals and the Akaike Information Criterion (Yamaoka et al., 1978). The intrinsic clearance (CL_{int}) is given as V_{max}/K_m for single enzyme kinetics and $V_{max1}/K_{m1}+V_{max2}/K_{m2}$ for the two-isoenzyme system.

JPET Fast Forward. Published on August 10, 2005 as DOI: 10.1124/jpet.105.090928
This article has not been copyedited and formatted. The final version may differ from this version.

RESULTS

Identification of metabolites of OME enantiomers. Control incubations showed that the metabolite formation required microsomal enzymes and NADPH. In HLM, four oxidized metabolites were formed after incubation with OME enantiomers. Three of the metabolites were identified as 5'-*O*-desmethylOME, 5-OH-OME and OME sulfone by comparing them with synthetic reference compounds. The other hydroxylated metabolite was identified as 3-OH-OME in accordance with previous studies (Weidolf, Data on file). rCYP3A4 catalyzed the formation of all four metabolites, while rCYP2C19 only catalyzed 5-hydroxylation and 5'-*O*-demethylation.

Stereoselective metabolism kinetics of omeprazole enantiomers in HLM and recombinant CYP2C19 and 3A4. Eadie-Hofstee plots for the formation kinetics of the metabolites of OME in HLM (plots not shown) indicated that 3-hydroxylation and sulfoxidation were performed by a single enzyme, whereas 5'-*O*-demethylation and 5-hydroxylation appeared to involve multiple P450 enzymes. Consequently, the experimental data were evaluated using the single or two-enzyme Michaelis-Menten models that best described the kinetics for the individual metabolites. Pronounced enantioselectivity for 5-hydroxylation, 5'-*O*-demethylation and sulfoxidation was observed after incubation of the individual enantiomers in HLM (Table 1). Regarding 5-hydroxylation, *R*-OME showed a 5-fold lower K_{m1} than the *S*-isomer in HLM and the corresponding CL_{int} was 7-fold higher. On the other hand, *S*-OME exhibited 2- and 3-fold higher CL_{int} of 5'-*O*-demethylation and sulfoxidation, respectively, than for the *R*-isomer. Consequently, the total CL_{int} of *R*-OME in HLM was 2.2-fold higher than that of the *S*-isomer. Similar stereoselectivity

JPET Fast Forward. Published on August 10, 2005 as DOI: 10.1124/jpet.105.090928
This article has not been copyedited and formatted. The final version may differ from this version.

was also observed when the pseudoracemate (50/50) was used as substrate, with the result that the total apparent CL_{int} of *R*-OME in HLM was 1.5-fold higher than that of *S*-isomer. The values of CL_{int} for OME racemate, i.e. the equimolar mixture of the *R*- and *S*-enantiomers, were in between the values of those for the individual enantiomers (Table 1). In agreement with previous data (Äbelö et al., 2000), the enzyme kinetic parameters obtained from rCYP2C19 and rCYP3A4 confirmed that the metabolic reactions of OME enantiomers obey simple Michaelis-Menten kinetics and these two enzymes are the main contributors to the stereoselective metabolism of the OME enantiomers. CYP2C19 favors *R*-OME for 5-hydroxylation and *S*-OME for 5'-*O*-demethylation, while CYP3A4 favors *R*-OME for 5-hydroxylation and *S*-OME for 5'-*O*-demethylation as well as 3-hydroxylation and sulfoxidation. When OME pseudoracemate was incubated in HLM or rCYPs, the apparent K_m^{app} and $V_{\max}^{app}$ values for the formation of each metabolite from the enantiomers were lower as compared to incubation with the individual enantiomers, indicating interactions between the two enantiomers. Representative Michaelis-Menten curves are depicted in Fig 2-4.

Results obtained after incubation of *S*-[$^{13}C_7$]OME in a separate experiment were identical to those obtained after incubation of the unlabelled *S*-enantiomer (data not shown). Therefore, isotope effects on the formation of metabolites of the labeled *S*-isomer could be excluded.

Inhibition studies. The inhibition potential of one OME enantiomer on the metabolic reactions of its optical antipode was investigated in HLM and rCYP2C19 and 3A4 using unlabelled *R*-OME and ^{13}C-labelled *S*-OME as substrate and inhibitor, respectively, and vice versa. Formation of unlabelled

JPET Fast Forward. Published on August 10, 2005 as DOI: 10.1124/jpet.105.090928
This article has not been copyedited and formatted. The final version may differ from this version.

and labeled metabolites from *R*- and *S*-[$^{13}C_7$]OME was measured separately. The apparent inhibition constants (K_i) for the formation of each metabolite of the OME enantiomers were calculated using the competitive inhibition model that provided the best fit. The results are summarized in Table 2. Figure 5 shows Dixon plots for the inhibition of *R*- or *S*-[$^{13}C_7$]OME 5-hydroxylase activities by their respective optical antipode in HLM and rCYP2C19.

R-OME 5-hydroxylation and 5'-*O*-demethylation activities were inhibited by the *S*-isomer in HLM exhibiting the K_i values of 11.3 and 27.9 μM, respectively, which is in agreement with that obtained in rCYP2C19 (11.6 and 13.3 μM, respectively). This suggests that these two metabolic reactions of *R*-OME are mainly catalyzed by CYP2C19 and are competitively inhibited by the *S*-isomer. The inhibitory effect of *R*-OME on the 5-hydroxylation and 5'-*O*-demethylation of *S*-[$^{13}C_7$]OME, however, was much less potent in HLM (K_i values of 42.1 and 28.9 μM, respectively) than in rCYP2C19 (K_i values of 1.2 and 1.3 μM, respectively). The inhibitory potency of *R*-OME on the 3-hydroxylation and sulfoxidation of *S*-[$^{13}C_7$]OME was poorer than that of *S*-OME on the same reactions of the *R*-isomer, in both rCYP3A4 and HLM. The CYP3A4 catalyzed 5-hydroxylation and 5'-*O*-demethylation of the OME enantiomers was poorly affected by their antipodes, exhibiting K_i values over 60 μM.

Competitive interaction model of enzyme kinetics of OME enantiomers in racemate. The OME enantiomers interacted competitively on CYP2C19 and 3A4. Predictions of their respective enzyme kinetics in racemate catalyzed by the single enzymes, rCYP2C19 or rCYP3A4, were performed based on the kinetic parameters of the individual OME enantiomers

JPET Fast Forward. Published on August 10, 2005 as DOI: 10.1124/jpet.105.090928
This article has not been copyedited and formatted. The final version may differ from this version.

and the kinetic model for competitive interaction between enantiomers in a racemic substrate (Kim et al., 1993) (equations are given in Materials and Methods). The predicted values of the enzyme kinetics (apparent K_m^{app}, $V_{\max}^{app}$ and CL_{int}^{app}) for the individual enantiomers in the racemic mixture were in good agreement with those observed when analyzed stereoselectively in a pseudoracemate incubation (Table 1 and Fig. 6), giving reduced apparent $V_{\max}^{app}$ and K_m^{app} that resulted in unchanged intrinsic clearances for the enantiomers in the pseudoracemate compared with those of the enantiomers when incubated individually. The most striking effect was the over 7-fold decrease in V_{max} and K_m of *S*-OME 5-hydroxylation in the presence of equal amounts of *R*-OME in rCYP2C19, which is consistent with the predicted values given by the competitive interaction model (Table 1). The *R/S* ratios of the predicted and observed apparent $V_{\max}^{app}$ of 5-hydroxylation (11.8 and 12.8, respectively) agreed with the ratio of their intrinsic clearances for the individual incubation of the enantiomers as well as for the pseudoracemate (value of 11.8), as predicted by eqs. 5 and 7. The predicted kinetics of *R*- and *S*-OME 5-hydroxylation by rCYP2C19 in the presence of their respective antipode at different concentrations is illustrated in Figure 6. The solid line represents the enzyme kinetics of the substrate in the presence of equal concentrations of the competitive inhibitor in the incubations, where the apparent $V_{\max}^{app}$ values of both enantiomers are lower. Most data points predicted by the single enzyme Michaelis-Menten kinetic model (Fig. 6) fit well with the observed data in the pseudoracemate (Fig. 3) except that the activities of *R*-OME was somewhat lower than the predicted values at concentrations higher than 60 μM.

JPET Fast Forward. Published on August 10, 2005 as DOI: 10.1124/jpet.105.090928
This article has not been copyedited and formatted. The final version may differ from this version.

However, when the pure *R*-OME enantiomer was incubated the Michealis-Menten kinetic model describes the 5-hydroxylase activity well even at high concentration. The same observation was also found for *S*-OME 5'-*O*-demethylation in the pseudoracemate compared to the individual enantiomer in rCYP2C19. Whether these deviations are due to enantiomer/enantiomer interactions only, or if other mechanisms also contribute, remains to be studied.

The ratios for the metabolite formation velocities (v_R/v_S) of the enantiomers at different substrate concentrations are shown in Figure 7. 5'-*O*-demethylation by rCYP2C19 exhibited the highest stereoselectivity and the formation of 3-OH-OME the lowest stereoselectivity in HLM. When the individual enantiomers were incubated with rCYP2C19, the v_R/v_S ratio for the formation of 5-OH-OME decreased significantly as substrate concentrations were increased, whereas this decrease was not prominent in HLM or rCYP3A4. As predicted by the competitive interaction model, the v_R/v_S ratios of the single rCYP catalyzed reactions were independent of the substrate concentration when the pseudoracemate was studied but not necessarily with the same pattern when the enantiomers were incubated individually (Fig. 7). When incubated as a pseudoracemate in HLM, the v_R/v_S ratios of OME 3-hydroxylation and sulfoxidation were also less affected by the substrate concentration, suggesting that a single enzyme was involved in the reaction. However, the v_R/v_S ratios for OME 5-hydroxylation and 5'-*O*-demethylation changed with the substrate concentration, indicating the involvement of multiple enzymes with different enzyme affinities and stereoselectivities. In

JPET Fast Forward. Published on August 10, 2005 as DOI: 10.1124/jpet.105.090928
This article has not been copyedited and formatted. The final version may differ from this version.

agreement with the prediction, at low substrate concentrations the v_R/v_S ratios of all the four metabolic reactions of OME were close to the *R/S* ratio of the respective CL_{int} values for the enantiomers individually, as well as for the pseudoracemate.

Relative contribution of CYP2C19 and CYP3A4 to omeprazole 5-hydroxylase and 5'-*O*-demethylase activities in HLM. Because two enzyme systems are involved in OME 5-hydroxylation and 5'-*O*-demethylation in HLM, the relative contribution of CYP2C19 and 3A4 for these two metabolic reactions of *S*- and *R*-OME were estimated using enzyme kinetic parameters obtained from rCYPs with the RAFs obtained previously (Li et al., 2003) (Fig. 8). According to this approach, CYP2C19 was found to be dominant over CYP3A4 in catalyzing 5-hydroxylation and 5'-*O*-demethylation of the individual OME enantiomers at low substrate concentration. However, with increasing substrate concentration, the contribution of CYP2C19 decreased continuously with a concomitant increase in the contribution by CYP3A4. For *R*-OME 5-hydroxylation, the contribution of CYP2C19 decreased from 89% at 1 μM to 41% at 128 μM, and for *S*-OME 5-hydroxylation the change was from 79% to 51% over the same concentration range. Furthermore, the relative contribution of the two rCYPs on the metabolism of one enantiomer in the presence of its antipode was studied using OME pseudoracemate. Interestingly, the relative contribution of CYP2C19 for *S*-[$^{13}C_7$]OME 5-hydroxylation decreased from 76% to 19% at increasing substrate concentrations with equimolar concentrations of *R*-OME, and the contribution of CYP3A4 increased up to 80%, with a switch point for CYP3A4 to dominate the metabolic activity over CYP2C19 at equimolar enantiomer concentrations

of about 8 μM. A less but significant effect was also observed on *S*-[$^{13}C_7$]OME 5'-*O*-demethylation. However, the CYP contribution profiles did not change significantly for 5-hydroxylation and 5'-*O*-demethylation of *R*-OME in the presence of *S*-[$^{13}C_7$]OME in the pseudoracemic mixture.

JPET Fast Forward. Published on August 10, 2005 as DOI: 10.1124/jpet.105.090928
This article has not been copyedited and formatted. The final version may differ from this version.

DISCUSSION

The administration of racemic drugs has received considerable attention over the past decade (Hutt and Tan, 1996; Islam et al., 1997). Differences in overall disposition of enantiomers can arise from stereoselective metabolism and inhibition of each other's metabolism. In the latter case, the enantiomers can compete for the same metabolizing enzymes, which affect elimination and may modify drug action. Although most chiral drugs are administered as the racemate, a few examples of interactions between enantiomers have been described (Kroemer et al., 1996).

In this study, the v_R/v_S (or v_R^{app}/v_S^{app}) ratios of the metabolic reactions of OME enantiomers showed different profiles over the concentration range studied. According to Michaelis-Menten kinetics and the competitive interaction model, this ratio of the competing enantiomers can reflect the stereoselectivity and the affinity of the enantiomers to the enzymes. At low substrate concentration, this ratio is close to the ratio of the true $CL_{\text{int},R}/CL_{\text{int},S}$ by both individual enantiomers and the racemate and shows the enzyme stereoselectivity of the reaction. When the ratio is not changing with the substrate concentration, it indicates that the two enantiomers have similar affinities to the enzymes ($K_{m,R}$ is similar to $K_{m,S}$) (e.g. v_R^{app}/v_S^{app} of the racemate is constant in rCYPs, where $K_{m,R}^{app} = K_{m,S}^{app}$). However, when the ratio is changing it suggests that the enantiomers have different affinities to one enzyme or that multiple enzymes are involved. In HLM, the v_R/v_S ratios of 5-hydroxylation for the individual enantiomers changed significantly in comparison with the other

reactions over the studied concentration range, indicating that the difference in the enantiomers' affinities and stereoseletivities for the 5-hydroxylation enzymes is greater than for the other reactions.

In vivo studies on the stereoselectivity of the OME enantiomers have been reported previously. *R*-OME showed higher in vivo clearance than *S*-OME with *R/S* clearance ratios (*CL/F*) of 1.4 and 1.9 after oral dosing of racemic OME and the individual enantiomers, respectively, in CYP2C19 EMs (Tybring et al., 1997; Andersson et al., 2001). However, an opposite stereoselectivity was observed for CYP2C19 PMs in both studies, with a clearance ratio (*R/S*) of 0.6 after administration of racemic OME, as well as the enantiomers individually. In our study, the total in vitro CL_{int} values for *R*-OME were 1.5- and 2.2-fold higher than for *S*-OME in the incubations with the pseudoracemate and individual enantiomers, respectively, which are in agreement with those from the in vivo studies in EMs. In CYP2C19 PMs, the clearance of OME is significantly reduced and, in these subjects, CYP3A4 may function as an alternative OME-metabolizing enzyme (Tybring et al., 1997). Our in vitro studies on rCYP3A4 showed that the *R/S* ratio of the total intrinsic clearance was 0.4 (Table 1), which agrees with the value of 0.6 observed in vivo in CYP2C19 PMs.

Clinical data on racemic OME (20 mg) indicate that the plasma concentrations of OME sulfone were about 20-50% of those for 5-OH-OME in EMs after oral administration (Tybring et al., 1997; Furuta et al., 1999). This in vivo observation is consistent with the in vitro microsomal data at OME racemate concentrations below 5 µM, where CYP2C19 is the predominant enzyme involved. At high OME racemate concentration, the formation rate of

OME sulfone is almost comparable with that of 5-hydroxylation, where the contribution of CYP3A4 is significant. For the individual incubation of *S*-OME in HLM, however, the relative formation rate of 5-OH-OME to that of the sulfone did not change significantly with increasing *S*-OME concentration. The sulfone is the major metabolite formed, with concentrations about 2-fold higher than those of 5-OH-OME in the *S*-OME range from 1 μM to 100 μM. This result is in good agreement with an in vivo study, where the plasma concentration (C_{max}) of OME sulfone was about 2.5-fold that of 5-OH-OME after a single oral dose of 40 mg esomeprazole (Hassan-Alin et al., 2000). This finding suggests that the metabolism of *S*-OME is less dependent on CYP2C19.

The inhibition potency of *R*-OME on the 5'-*O*-demethylation and 5-hydroxylation of *S*-OME was greater in rCYP2C19 than in HLM, whereas no such difference was seen for the inhibition by *S*-OME on the 5'-*O*-demethylation and 5-hydroxylation of *R*-OME. An explanation for this difference in the inhibition pattern might be the higher contribution of CYP3A4 to 5'-*O*-demethylation and 5-hydroxylation of *S*-OME than *R*-OME in HLM. Figure 8 shows that CYP3A4 becomes increasingly important for *S*-OME 5-hydroxylation and 5'-*O*-demethylation when incubated with its antipode, as opposed to when incubated alone. Thus, when the metabolism of *S*-OME by CYP2C19 in HLM is inhibited by *R*-OME, the metabolism of *S*-OME is switched to CYP3A4, on which the inhibitory effect of *R*-OME is less significant. For *R*-OME, this difference between the relative contribution of enzymes when comparing racemate and enantiomers was not so significant.

The results presented in this study indicate that the enantiomers are competing for the same P450 isoforms, with evidence for: 1) lower V_{max} values for all four metabolic reactions when incubated as pseudoracemate as compared with those for the individual enantiomers; 2) enzyme kinetics of the enantiomers in pseudoracemate which fit the model of competitive interaction between enantiomers; and 3) both enantiomers were shown to be competitive inhibitors of each other's metabolism. The phenomenon of mutual competition between the enantiomers for the active site(s) has been reported, e.g. the enantiomer interactions of propafenone 5-hydroxylation by CYP2D6 (Kroemer et al., 1991), cisapride *N*-dealkylation by CYP3A4 (Desta et al., 2000), and flurbiprofen 4'-hydroxylation by CYP2C9 (Tracy et al., 1995). These in vitro studies may reflect an in vivo situation, in which stereoselective first-pass metabolism leads to a ratio of the enantiomers different from unity in the systemic circulation. As a consequence, the ratio of substrate to inhibitor in this system will vary with time. Such interactions may be of clinical relevance if, as in the case of propafenone, the enantiomers differ in terms of pharmacological potency and, therefore, inhibition of metabolism of one enantiomer by its optical antipode may modulate the net pharmacological effect of the drug. In the case of OME, for which the proton pump inhibiting properties of the enantiomers are equal, the knowledge of the pharmacokinetic properties for the single enantiomer *vs.* those of the racemate is important for the understanding of the relationship between the given dose and the pharmacological effect.

The CYP2C19-dependent polymorphic metabolism of PPIs in humans is well known (McColl and Kennerley, 2002). The exposure of *S*-OME, when

administered alone, as compared with the OME exposure after dosing with the racemate, is higher in EMs but lower in PMs. Thus, dosing of the pure *S*-isomer of OME contributes to a decreased interindividual variability between EMs and PMs. The in vivo and/or in vitro stereoselective metabolism of other PPIs such as pantoprazole (Tanaka et al., 1997; Tanaka et al., 2001) and lansoprazole (Katsuki et al., 1996; Katsuki et al., 2001; Kim et al., 2002) has also been reported. After doses of racemic pantoprazole, marked stereoselective disposition was observed only in CYP2C19 PMs with (+)/(–) clearance ratios (*CL/F*) of 1.25 and 0.29 in EMs and PMs, respectively (Tanaka et al., 2001). The clearance of (+)-pantoprazole was suggested to be related to CYP2C19 to a greater extent than the disposition of the (–)-enantiomer, which is similar to the situation for OME. For lansoprazole, after racemate dosing, the *R*(+)/*S*(–) clearance ratio of the enantiomers was not significantly different between EMs and PMs, with values of 0.15 and 0.19, respectively (Kim et al., 2002). It was suggested that, unlike OME, the enantioselective disposition of lansoprazole is less influenced by CYP2C19 genetic polymorphism and that a likely contributing factor is its stereoselective protein binding. However, with the reported stereoselective metabolism of the pantoprazole and lansoprazole enantiomers, catalyzed by the same CYP isoforms as OME, these compounds may well exhibit enantiomer/enantiomer interactions similar to those of OME.

In conclusion, we have shown enantiomer/enantiomer interactions for the formation of four metabolites of *R*- and *S*-OME, i.e. 5- and 3-OH-OME, 5'-*O*-desmethylOME and OME sulfone. The in vitro experiments demonstrated that the inhibition mechanism for these interactions is competitive and that the

JPET Fast Forward. Published on August 10, 2005 as DOI: 10.1124/jpet.105.090928
This article has not been copyedited and formatted. The final version may differ from this version.

metabolism of *R*- and *S*-OME by CYP2C19 and CYP3A4 is stereoselective. Our analyses indicate that the enantiomer/enantiomer interaction does not significantly change the clearances of the enantiomers in the racemate as compared to those of the individual enantiomers. With regard to the equal proton pump inhibiting properties of the OME enantiomers, one might expect the enantiomer/enantiomer interaction during OME racemate therapy to be of little pharmacodynamic relevance. However, our study suggests that the use of the pure *S*-enantiomer of OME should be favorable in clinical therapy, providing a clearer metabolic profile and better predictability regarding pharmacokinetics and efficacy in comparison with the racemate.

Acknowledgements

We gratefully thank Dr. Ulf Bredberg and Dr. Tommy Andersson (AstraZeneca Pharmaceuticals LP) for fruitful discussions on this manuscript.

References

Äbelö A, Andersson T, Antonsson M, Naudot A, Skanberg I and Weidolf L (2000) Stereoselective metabolism of omeprazole by human cytochrome P450 enzymes. *Drug Metab Dispos* **28**:966-972.

Andersson T, Hassan-Alin M, Hasselgren G, Rohss K and Weidolf L (2001) Pharmacokinetic studies with esomeprazole, the (S)-isomer of omeprazole. *Clin Pharmacokinet* **40**:411-426.

Crespi C (1995) Xenobiotic-metabolizing human cells as tools for pharmacological and toxicological research. *Adv Drug Res* **26**:179-235.

Desta Z, Soukhova N, Mahal S and Flockhart D (2000) Interaction of cisapride with the human cytochrome P450 system: metabolism and inhibition studies. *Drug Metab Dispos* **28**:789-800.

Ernster L, Siekevitz P and Palada G (1962) Enzyme-structure relationships in the endoplasmic reticulum of rat liver. *J Cell Biol* **15**:541-562.

Furuta T, Ohashi K, Kobayashi K, Iida I, Yoshida H, Shirai N, Takashima M, Kosuge K, Hanai H, Chiba K, Ishizaki T and Kaneko E (1999) Effects of clarithromycin on the metabolism of omeprazole in relation to CYP2C19 genotype status in humans. *Clin Pharm Therap* **66**:265-274.

Hassan-Alin M, Andersson T, Bredberg E and Rohss K (2000) Pharmacokinetics of esomeprazole after oral and intravenous administration of single and repeated doses to healthy subjects. *Eur J Clin Pharmacol* **56**:665-670.

Hutt A and Tan S (1996) Drug chirality and its clinical significance. *Drugs* **52**:1-12.

Islam M, Mahdi J and Bowen I (1997) Pharmacological importance of stereochemical resolution of enantiomeric drugs. *Drug Safety* **17**:149-165.

Katsuki H, Hamada A, Nakamura C, Arimori K and Nakano M (2001) Role of CYP3A4 and CYP2C19 in the stereoselective metabolism of lansoprazole by human liver microsomes. *Eur J Clin Pharmacol* **57**:709-715.

Katsuki H, Yagi H, Arimori K, Nakamura C, Nakano M, Katafuchi S, Fujioka Y and Fujiyama S (1996) Determination of R(+)- and S(-)-lansoprazole using chiral stationary- phase liquid chromatography and their enantioselective pharmacokinetics in humans. *Pharmaceut Res* **13**:611-615.

Kim K-A, Shon J-H, Park J-Y, Yoon Y-R, Kim M-J, Yun D-H, Kim M-K, Cha I-J, Hyun M-H and Shin J-G (2002) Enantioselective disposition of lansoprazole in extensive and poor metabolizers of CYP2C19. *Clin Pharmacol Ther* **72**:90-99.

Kim M, Shen D, Eddy A, Nelson W and Roskos L (1993) Inhibition of the enantioselective oxidative metabolism of metoprolol by verapamil in human liver microsomes. *Drug Metab Dispos* **21**:309-317.

Kroemer H, Fischer C, Meese C and Eichelbaum M (1991) Enantiomer/enantiomer interaction of (S)- and (R)-propafenone for cytochrome P450IID6-catalyzed 5-hydroxylation: in vitro evaluation of the mechanism. *Mol Pharmacol* **40**:135-142.

Kroemer H, Fromm M and Eichelbaum M (1996) Stereoselectivity in drug metabolism and action: effects of enzyme inhibition and induction. *Ther Drug Monit* **18**:388-392.

Li X, Andersson T, Ahlström M and Weidolf L (2004) Inhibitory Effects of the Proton Pump Inhibiting Drugs Omeprazole, Esomeprazole, Lansoprazole, Pantoprazole and Rabeprazole on Human Cytochrome P450 Activities. *Drug Metab Dispos* **32**:821-827.

Li X, Björkman A, Andersson T, Gustafsson L and Masimirembwa C (2003) Identification of human cytochrome P450s that metabolise anti-parasitic drugs and predictions of in vivo drug hepatic clearance from in vitro data. *Eur J Clin Pharmacol* **59**:429-442.

Lindberg P, Keeling D, Fryklund J, Andersson T, Lundborg P and Carlsson E (2003) Review article: esomeprazole - enhanced bio-availability, specificity for the

proton pump and inhibition of acid secretion. *Aliment Pharmacol Ther* **17**:481-488.

Lindberg P, Nordberg P, Alminger T, Brändström A and Wallmark B (1986) The mechanism of action of the gastric acid secretion inhibitor omeprazole. *J Med Chem* **29**:1327-1329.

Lowry O, Rosebrough N, Farr A and Randall R (1951) Protein measurement with the folin phenol reagent. *J Biol Chem* **193**:265-275.

Masimirembwa CM, Otter C, Berg M, Jönsson M, Leidvik B, Jonsson E, Johansson T, Bäckman A, Edlund A and Andersson TB (1999) Heterologous Expression and Kinetic Characterization of Human Cytochromes P-450: Validation of a Pharmaceutical Tool for Drug Metabolism Research. *Drug Metab Dispos* **27**:1117-1122.

McColl K and Kennerley P (2002) Proton pump inhibitors-differences emerge in hepatic metabolism. *Digest Liver Dis* **34**:461-467.

Miner P, Katz P, Chen Y and Sostek M (2003) Gastric acid control with esomeprazole, lansoprazole, omeprazole, pantoprazole, and rabeprazole: a 5-way crossover study. *Am J Gastroenterol* **98**:2616-2620.

Renberg L, Simonsson R and Hoffmann K (1989) Identification of two main urinary metabolites of [14C]omeprazole in humans. *Drug Metab Dispos* **17**:69-76.

Störmer E, von Moltke L and Greenblatt D (2000) Scaling drug biotransformation data from cDNA-expressed cytochrome P-450 to human liver: a comparison of relative activity factors and human liver abundance in studies of mirtazapine metabolism. *J Pharmacol Exp Ther* **295**:793-801.

Tanaka M, Ohkubo T, Otani K, Suzuki A, Kaneko S, Sugawara K, Ryokawa Y and Ishizaki T (2001) Stereoselective pharmacokinetics of pantoprazole, a proton pump inhibitor, in extensive and poor metabolizers of S-mephenytoin. *Clin Pharmacol Ther* **69**:108-113.

Tanaka M, Yamazaki H, Hakusui H, Nakamichi N and Sekino H (1997) Differential stereoselective pharmacokinetics of pantoprazole, a proton pump inhibitor in extensive and poor metabolizers of pantoprazole-A preliminary study. *Chirality* **9**:17-21.

Tracy T, Rosenbluth B, Wrighton S, Gonzalez F and Korzekwa K (1995) Role of cytochrome P450 2C9 and an allelic variant in the 4'-hydroxylation of (R)- and (S)-flurbiprofen. *Biochem Pharmacol* **49**:1269-1275.

Tybring G, Bottiger Y, Widen J and Bertilsson L (1997) Enantioselective hydroxylation of omeprazole catalyzed by CYP2C19 in Swedish white subjects. *Clin Pharmacol Ther* **62**:129-137.

Yamaoka K, Nakagawa T and Uno T (1978) of Akaike's information criterion (AIC) in the evaluation of linear pharmacokinetic equations. *J Pharmacokinet Biopharm* **6**:165-175.

Legends for Figures:

Figure 1. Structures of *S*- and *R*-omeprazole and the four oxidized metabolites. *, denotes the position of the [^{13}C]-labels.

Figure 2. Kinetics of 5- and 3-hydroxyomeprazole, 5'-*O*-desmethylomeprazole and omeprazole sulfone formation from omeprazole racemate and from *R*- and *S*-omeprazole enantiomers after individual or simultaneous incubation of *R*- and *S*-omeprazole in HLM. Each point represents the mean of duplicate measurements.

Figure 3. Kinetics of 5- hydroxyomeprazole and 5'-*O*-desmethylomeprazole formation from omeprazole racemate and from *R*- and *S*-omeprazole enantiomers after individual or simultaneous incubation of *R*- and *S*-omeprazole in rCYP2C19. Each point represents the mean of duplicate measurements.

Figure 4. Kinetics of 5- and 3-hydroxyomeprazole, 5'-*O*-desmethylomeprazole and omeprazole sulfone formation from omeprazole racemate and from *R*- and *S*-omeprazole enantiomers after individual or simultaneous incubation of *R*- and *S*-omeprazole in rCYP3A4. Each point represents the mean of duplicate measurements.

Figure 5. Dixon plots showing the inhibition of 5-hydroxylase activity for the omeprazole enantiomers by their respective optical antipodes in human liver microsomes (A and B) and rCYP2C19 (C and D). A and C show the inhibition of *R*-omeprazole 5-hydroxylation by *S*-[$^{13}C_7$]omeprazole; B and D show the inhibition of *S*-[$^{13}C_7$]omeprazole 5-hydroxylation by *R*-omeprazole, respectively.

Figure 6. Estimated kinetics of 5-hydroxylation of *S*-omeprazole (top) and *R*-omeprazole (bottom) in rCYP2C19 in the presence of their respective antipode. Calculation was based on the enzyme kinetics of competitive substrates/inhibitors and the corresponding enzyme kinetic parameters listed in Table 1 (see description in text). The substrate concentrations were 1, 2, 4, 8, 16, 32, 64, and 128 µM. The solid lines show the estimated Michaelis-Menten curves of *S*- or *R*-omeprazole 5-hydroxylation activity in the presence of equal amounts of the optical antipode.

Figure 7. Ratios for the formation velocities (v_R/v_S) of 5'-*O*-desmethylomeprazole, 5-hydroxyomeprazole, 3-hydroxyomeprazole and omeprazole sulfone after incubation of the individual enantiomers or pesudoracemates in human liver microsomes and recombinant CYP2C19 and 3A4.

Figure 8. Relative contributions of CYP 2C19 and 3A4 to the formation of 5-hydroxyomeprazole and 5'-*O*-desmethylomeprazole of the *R*- and *S*-omeprazole enantiomers after separate or simultaneous incubation in HLM. Calculations were based on a relative activity factor (RAF) approach and on kinetic parameters given in Table 1.

Table 1 Kinetic parameters for omeprazole racemate and enantiomers with respect to the four major metabolic reactions, 5'-*O*-demethylation, 5- and 3-hydroxylation, and sulfoxidation, in human liver microsomes and rCYP2C19 and 3A4. The predicted apparent K_m and V_{max} values of OME enantiomers in racemate using a model of competitive interaction of enantiomers in racemate are shown in parentheses. The enantiomer data are obtained from incubation of enantiomers individually or in pseudoracemate. Units used are: K_m, μM; $V_{max, HLM}$, pmol/min/mg protein; $V_{max, rCYP}$, pmol/min/nmol P450; $CL_{int, HLM}$, μl/min/mg; $CL_{int, rCYP}$, μl/min/nmol P450.

Microsomes	Compound	5-Hydroxylation						5'-O-Demethylation						3-Hydroxylation				Sulfoxidation				Total	
		K_{m1}	K_{m2}	V_{max1}	V_{max2}	CL_{int}	R/S CL_{int}	K_{m1}	K_{m2}	V_{max1}	V_{max2}	CL_{int}	R/S CL_{int}	K_m	V_{max}	CL_{int}	R/S CL_{int}	K_m	V_{max}	CL_{int}	R/S CL_{int}	CL_{int}	R/S CL_{int}
HLM	Enantiomer																						
	R-OME	1.4	14	22	95	22.5	7.5	1.9	40	2.8	51	2.7	0.5	20	22	1.1	0.9	66	61	0.93	0.3	27.2	2.2
	S-OME	7.4	104	18	54	3.0		4.7	71	19.5	54	4.9		15	18	1.2		50	155	3.1		12.2	
	OME Racemate	2.9	35	26	65	11.1		1.9	44	5.4	59	4.2		17	19	1.1		35	91	2.6		19.0	
	Pseudoracemate																						
	R-OME	1.3	13	19	79	20.3	5.5	0.26	13	0.62	28	4.5	0.7	12	14	1.1	0.7	26	26	1.0	0.2	26.9	1.5
	S-[$^{13}C_7$]OME	1.8	24	4.3	30	3.7		1.9	21	8.9	38	6.6		11	16	1.5		17	97	5.7		17.4	
rCYP2C19	Enantiomer																						
	R-OME	1.6		2089		1324	11.8	3.4		167		49	0.06									1373	1.6
	S-OME	8.9		996		112		5.1		3874		753										865	
	OME Racemate	2.5		1732		680		2.5		1056.8		428										1108	
	Pseudoracemate																						
	R-OME	1.3		1568		1248	11.8	2.2		155		71	0.08									1319	1.3
	S-[$^{13}C_7$]OME	1.2		122		106		1.3		1195		893										999	
	Racemate (Predicted by competitive interaction model)																						
	R-OME	(1.3)		(1774)		(1324)	(11.8)	(2.1)		(100)		(49)	(0.06)									(1373)	(1.6)
	S-OME	(1.3)		(150)		(112)		(2.1)		(1546)		(753)										(865)	
rCYP3A4	Enantiomer																						
	R-OME	37		344		9.3	4.0	83		40		0.48	0.2	26		85	3.3	0.4	56.3	291	5.2	0.2	18	0.4
	S-OME	47		110		2.4		51		104		2.05		15		118	7.8		31.6	1009	31.9		44	
	OME Racemate	42		209		5.0		59		74		1.25		20		99	5.0		27	569	21.0		32	
	Pseudoracemate																						
	R-OME	37		171		4.7	3.0	54		20		0.36	0.2	16		30	1.8	0.4	36	131	3.7	0.2	11	0.4
	S-[$^{13}C_7$]OME	32		50		1.6		35		65		1.86		12		54	4.5		22	446	20.2		28	
	Racemate (Predicted by competitive interaction model)																						
	R-OME	(21)		(192)		(9.3)	(4.0)	(31)		(15)		(0.48)	(0.2)	(9.5)		(32)	(3.3)	(0.4)	(20)	(105)	(5.2)	(0.2)	(18)	(0.4)
	S-OME	(21)		(48)		(2.4)		(31)		(64)		(2.05)		(9.5)		(74)	(7.8)		(20)	(646)	(31.9)		(44)	

Table 2 Inhibition constant (K_i, Mean ± SD, μM) of *S*-[$^{13}C_7$]omeprazole and *R*-omeprazole to each other's 5'-*O*-demethylation, 5- and 3-hydroxylation and sulfoxidation in human liver microsomes, recombinant CYP2C19 and CYP3A4. All inhibitions were best described by the competitive inhibition model.

Metabolic reaction	*R*-Omeprazole (Substrate) *S*-[$^{13}C_7$]Omeprazole (Inhibitor)			*S*-[$^{13}C_7$]Omeprazole (Substrate) *R*-Omeprazole (Inhibitor)		
	HLM	rCYP2C19	rCYP3A4	HLM	rCYP2C19	rCYP3A4
5-hydroxylation	11.3 ± 0.57	11.6 ± 0.8	64.9 ± 3.5	42.1 ± 3.8	1.23 ± 0.10	118.6 ± 8.9
5'-*O*-demethylation	27.9 ± 1.5	13.3 ± 0.8	121.9 ± 7.3	28.9 ± 2.2	1.34 ± 0.11	175.5 ± 14.9
3-hydroxylation	20.3 ± 0.88	-	36.9 ± 2.0	38.1 ± 2.6	-	47.8 ± 3.4
Sulfone formation	15.6 ± 0.63	-	41.6 ± 2.3	91.0 ± 10.6	-	97.7 ± 7.9

Figure 1.

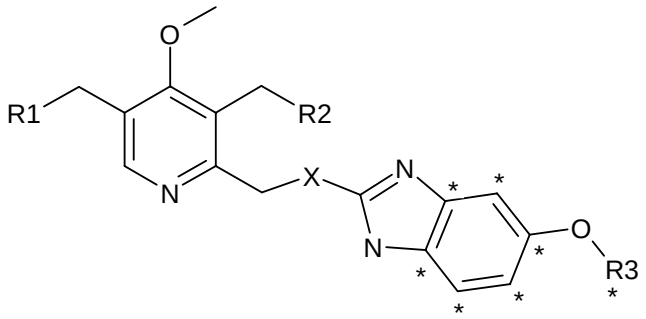

	R_1	R_2	R_3	X
S-Omeprazole	H	H	CH_3	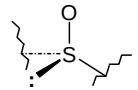
R-Omeprazole	H	H	CH_3	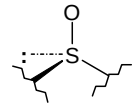
5'-O-Desmethylomeprazole	H	H	H	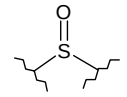
5-Hydroxyomeprazole	OH	H	CH_3	
3-Hydroxyomeprazole	H	OH	CH_3	
Omeprazole sulfone	H	H	CH_3	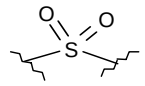

Figure 2.

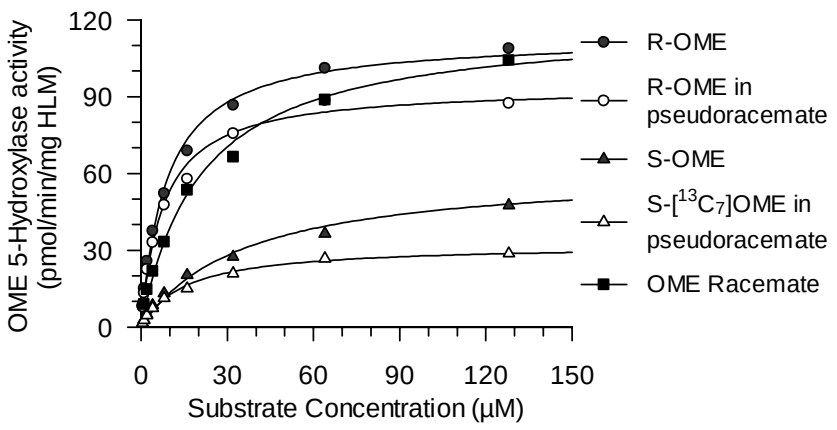

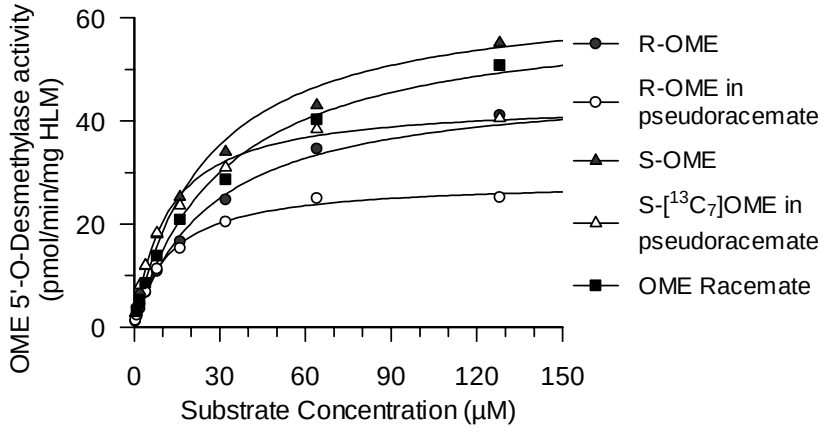

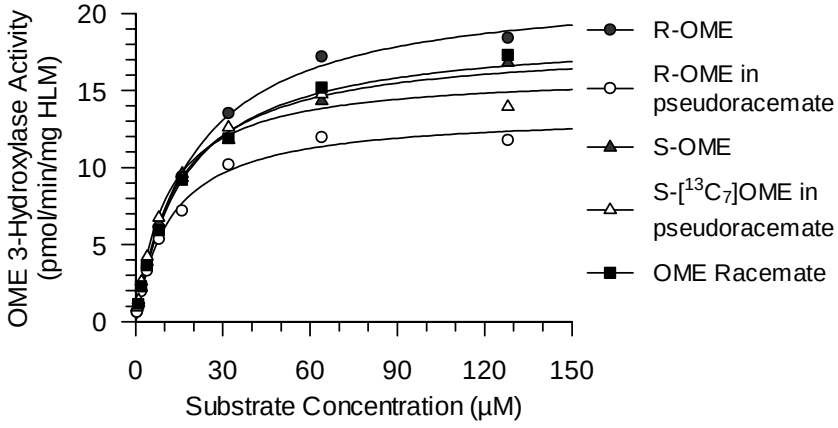

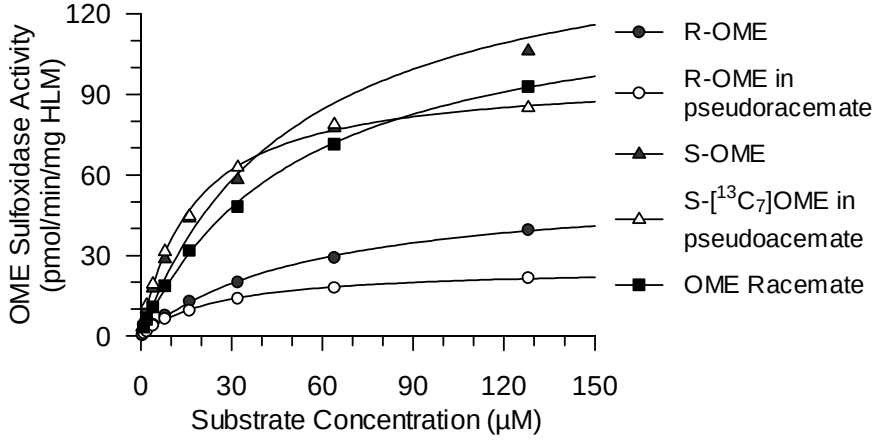

Figure 3.

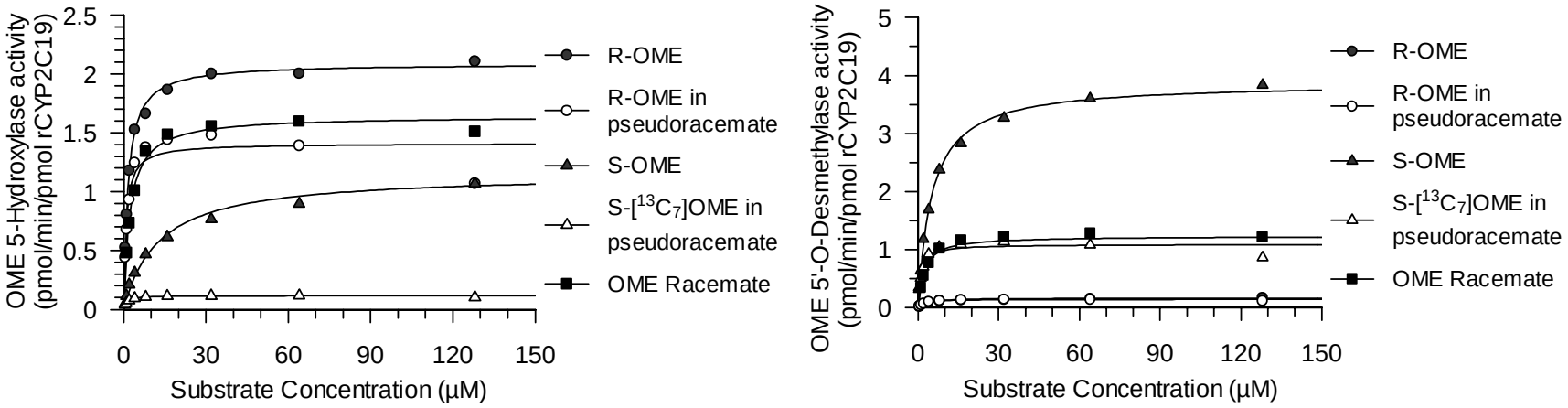

Figure 4.

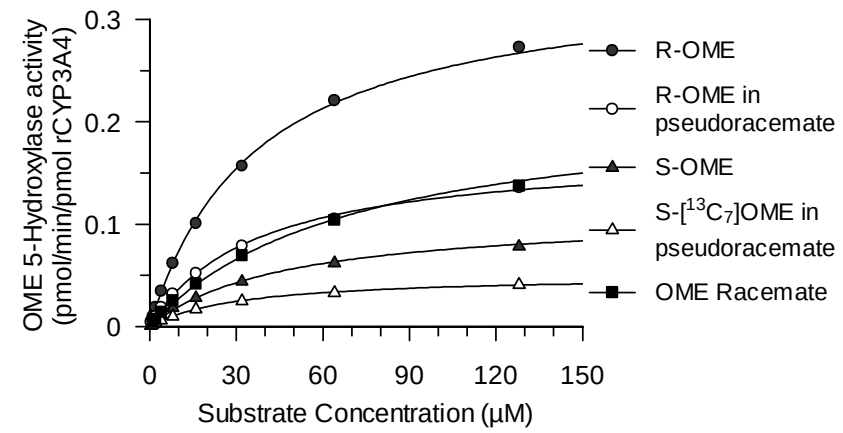

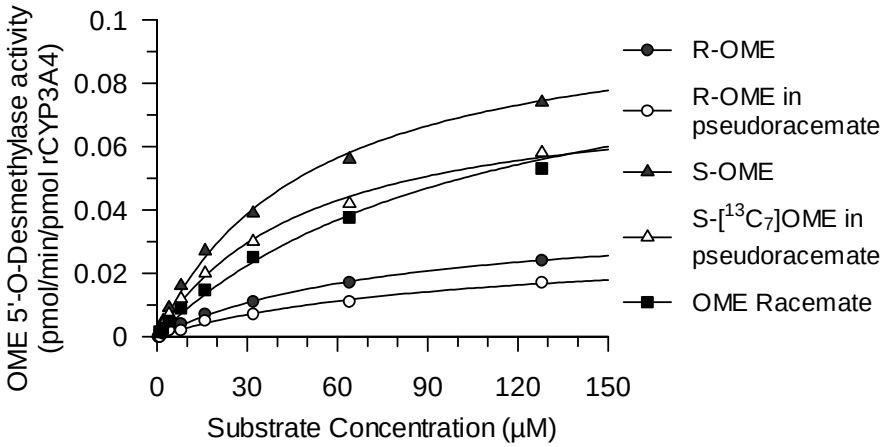

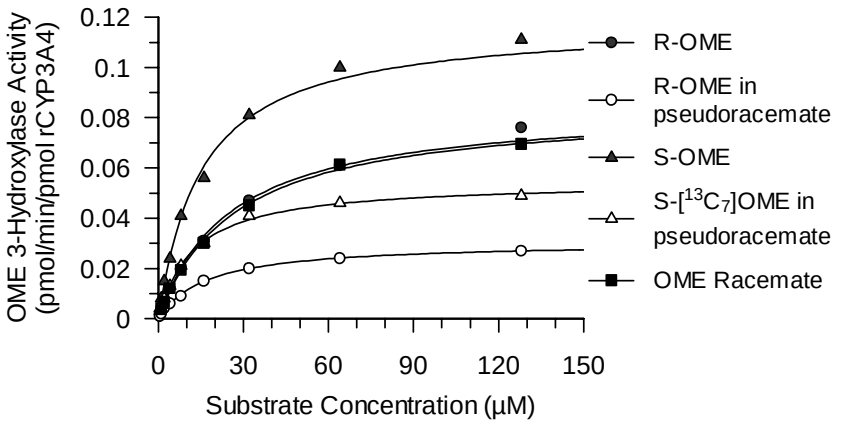

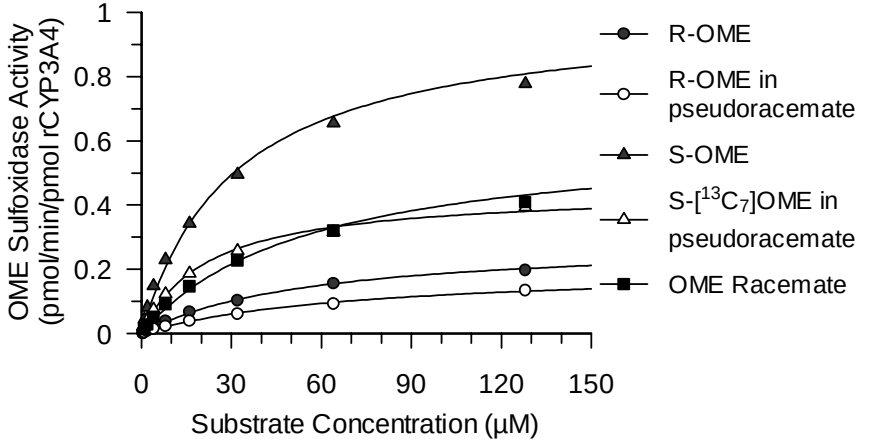

Figure 5.

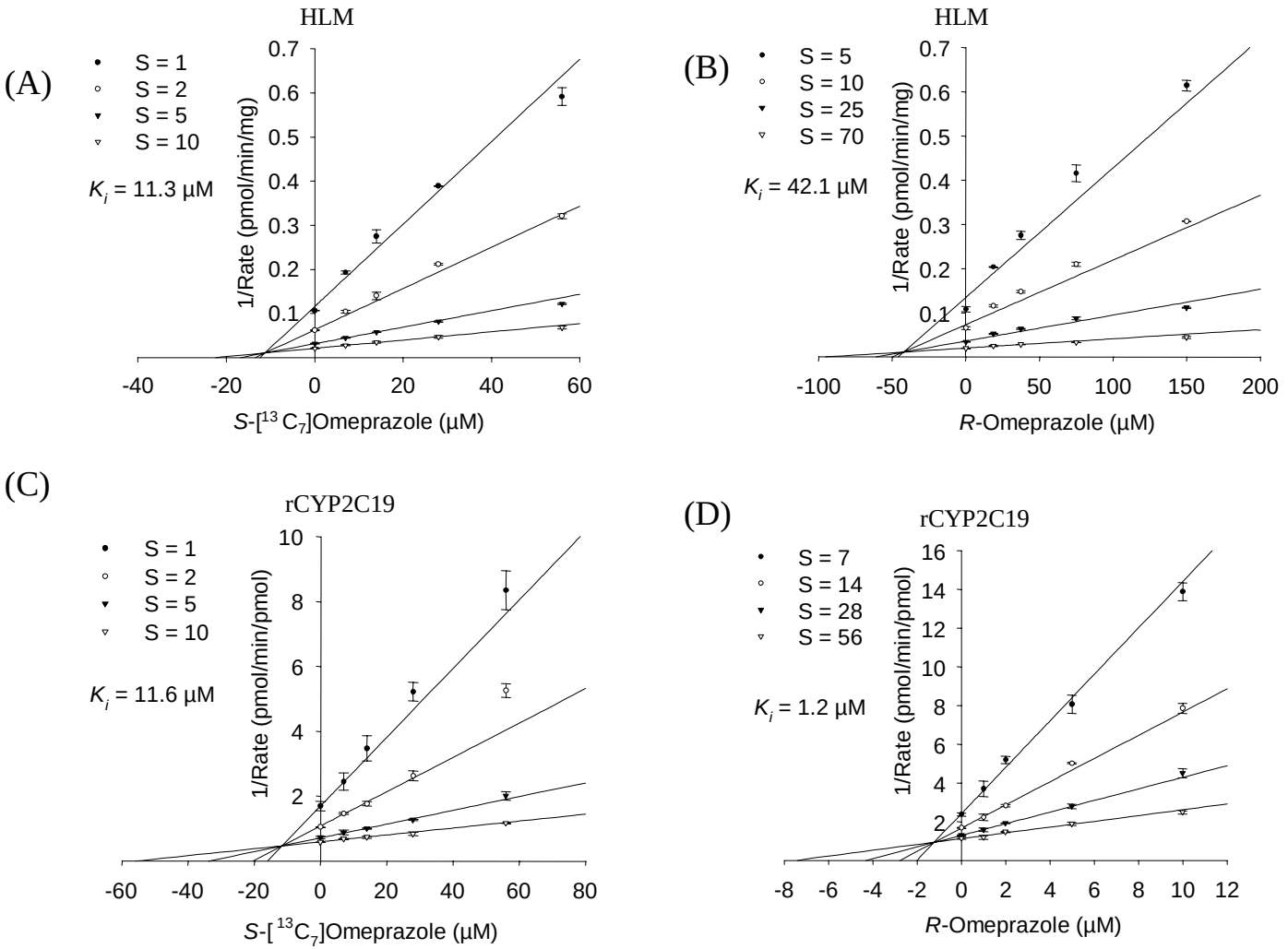

Figure 6.

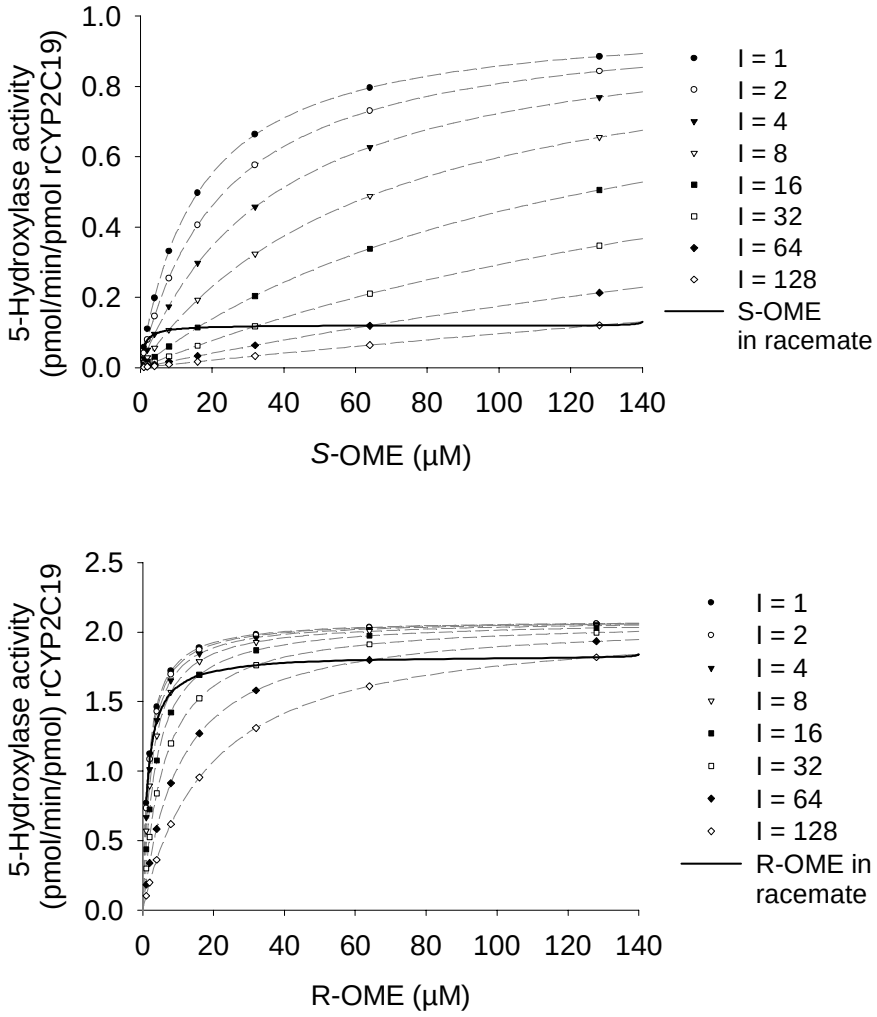

Figure 7.

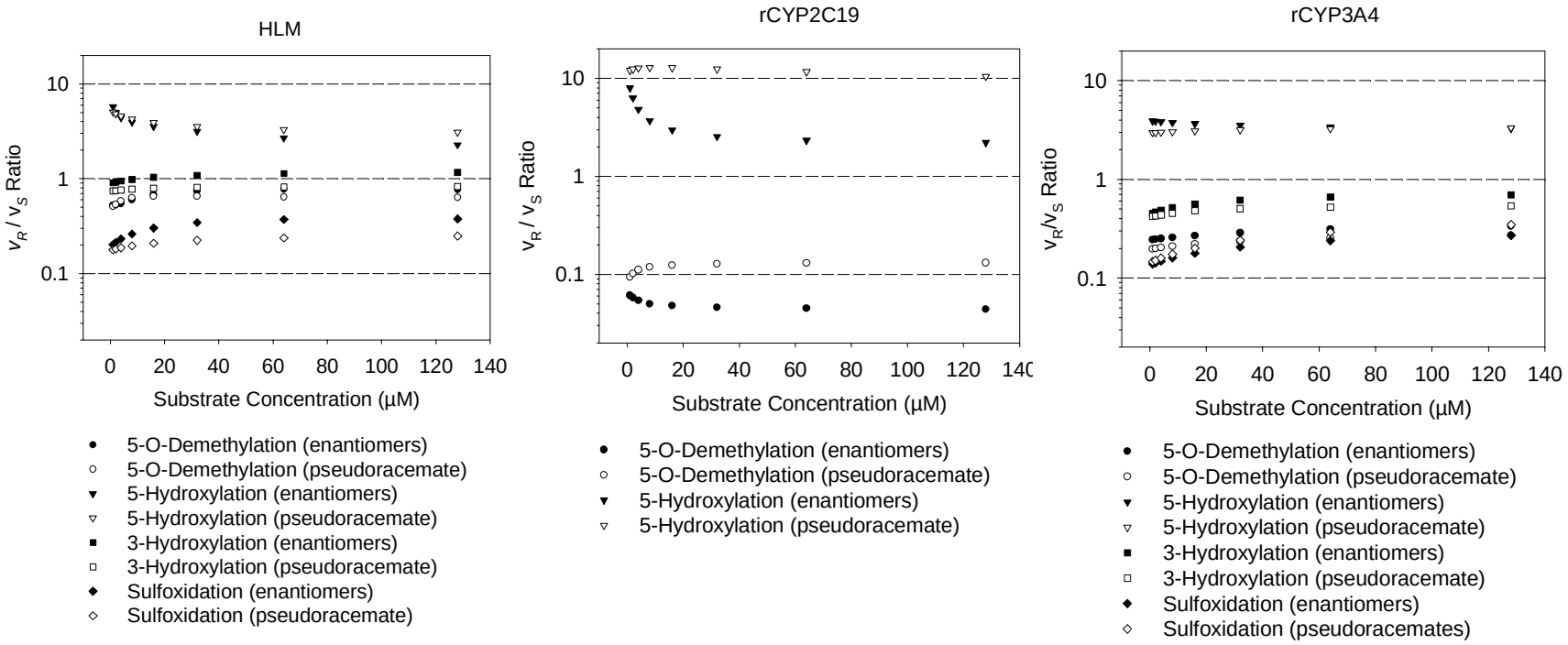

Figure 8.